# Peripapillary Atrophy Segmentation with Boundary Guidance

Mengxuan Li[1], He Zhao[1], Jie Xu[2], and Huiqi Li[1(✉)]

[1] Beijing Institute of Technology, Beijing, China
huiqili@bit.edu.cn
[2] Beijing Tongren Hospital, Beijing, China

**Abstract.** Peripapillary atrophy (PPA) is a clinical finding that reflects atrophy of the retinal layer and retinal pigment epithelium. It is very important to segment PPA area as it indicates the progress of eye diseases such as myopia and glaucoma, while it is a challenging task to segment PPA due to the irregular and ambiguous boundaries. In this paper, a boundary guidance deep learning method is introduced to segment PPA area to obtain precise shape. We propose a boundary guidance block together with a contour loss function to improve the PPA segmentation performance on boundaries. Our approach is evaluated on a clinical dataset. The F1-score, IOU and Hausdorff distance of our method performance is 80.06%, 67.29%, 5.4934 respectively. Compared with other methods, our method achieves the best performance both qualitatively and quantitatively. Our proposed method can work well on retinal images with narrow PPA even with small training set.

**Keywords:** Peripapillary atrophy (PPA) · Boundary guidance · Segmentation

## 1 Introduction

Peripapillary atrophy (PPA) is a clinical finding associated with chorioretinal thinning and disruption of the retinal pigment epithelium (RPE) in the area surrounding optic disc [1]. Clinical studies show that the presence of PPA often associates with myopia or glaucoma [2]. Therefore, monitoring PPA area is very helpful for myopia and glaucoma screening. In recent years, PPA segmentation has been investigated. Most methods segment the area of optic disc (OD) and PPA together (i.e. PPAOD) following by subtracting the OD region due to the difficulty of direct PPA segmentation [3]. Constraint on the shape of PPA or OD with a simple ellipse fitting is also considered in some work, but it leads to a limited improvement.

In this paper, we propose a novel deep learning method to segment PPA regions. Different from other work, we segment the PPA area directly, which reduces the model complexity compared with methods based on PPAOD subtraction. Furthermore, a new module is engaged in our network to provide the boundary guidance together with a contour constraint. The contributions of our approach can be summarized as follows. (1) A novel end-to-end PPA segmentation method is proposed to directly extract PPA region with a precise boundary in retinal images. (2) A boundary guidance block is


H. Fu et al. (Eds.): OMIA 2021, LNCS 12970, pp. 101–108, 2021.
https://doi.org/10.1007/978-3-030-87000-3_11

proposed to provide boundary information and work as a guidance for the network. (3) We utilize the contour loss to constrain the pixels around the boundary to further improve performance. (4) We have carried out extensive experiments with the clinical data to evaluate our approach. The results suggest that our approach achieves the superior performance compared with the state-of-the-art methods, and the performance is significantly improved even with small training set.

## 2 Related Work

Image segmentation is a classic problem in computer vision and there are many methods used in image segmentation, which are mainly divided into two categories: conventional segmentation methods and deep-learning based segmentation algorithms. Conventional segmentation methods vary from threshold-based, region-based and edge detection-based methods [4] to the wavelet analysis and active contour models [5]. With the development of deep learning, more and more convolutional neural network models have been proposed for segmentation task and achieve satisfactory performance, such as Unet [6] and SegNet [7].

Many methods are also proposed for retinal fundus image segmentation. Joshi et al. [8] proposed a novel OD segmentation method which integrates the local image information around each point of interest in multidimensional feature space. The method proposed by Yu et al. [9] used alternating sequential filtering (ASF) and morphological reconstruction to remove vessels and bright region distractors followed by level set model with both region information and local edge vector to segment OD. Bharkad et al. [10] proposed to segment the OD region using a combination of the equiripple low pass finite impulse response filter, thresholding, and grayscale morphological dilation and median filtering operation. Maninis et al. [11] proposed a network structure based on VGG network to segment both retinal vessel and OD. Wang et al. [12] proposed a coarse-to-fine pipeline which segments OD based on a U-net structure and the segmentation map from color funds images and corresponding grayscale vessel density maps.

As to retinal PPA segmentation, Lu et al. [3] proposed to extract PPA using region growing and modified Chan-Vese model with a shape constraint. This method searches for the local optimum, so it is seriously affected by initialization. Li et al. [13] used evenly-oriented radial lines to detect the candidate boundary points of OD and PPAOD, followed by outlier removal and ellipses fitting. The complicated illuminance situation around optical disk will lead to failure due to the unreliable point determination which relies on brightness curve on the radiation line. Chai et al. [14] proposed a novel PPA area segmentation using a multi-task fully convolutional Network, which simultaneously divided the OD and PPAOD regions and subtracted the two to obtain the final result.

## 3 Methodology

In this paper, we propose a boundary guidance PPA segmentation method, which contains a boundary guidance block with contour loss. These two components are helpful to learn

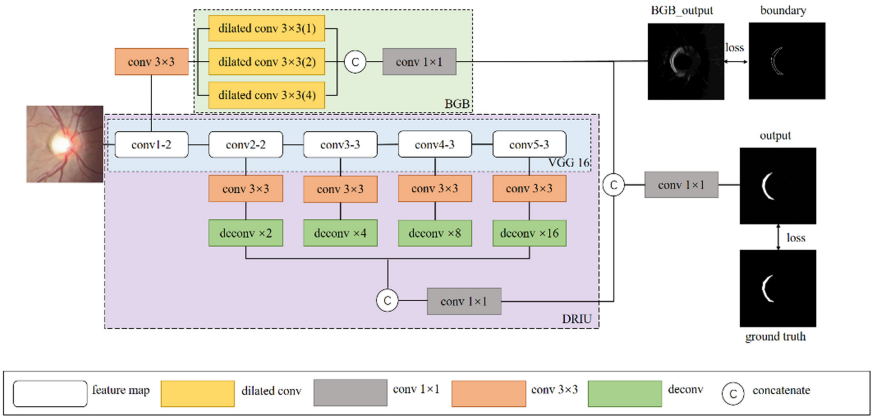


**Fig. 1.** The overview framework for PPA segmentation.

low-level boundary features and generate precise PPA shape. The overall architecture is illustrated in Fig. 1, which is designed based on backbone of DRIU [10]. Feature maps are extracted by VGG convolutional blocks and the proposed boundary guidance block, which are fused for the final segmentation result and provides an auxiliary boundary constraint. The boundary guidance block generates the refined feature maps maintaining boundary information. Combining the features from multiple scales provided by DRIU, the model can finally give the prediction of a full size segmentation map. In what follows, we will give detailed information on the main components of our approach.

### 3.1 Boundary Guidance Block (BGB)

Facing the problem of ambiguous shape in the segmentation map, we introduce a sharp-aware component to alleviate the issue by enhancing the power of boundary information extraction. If only the backbone network is used for segmentation, the segmentation map sometimes has a confusing shape at the boundary. Therefore, a boundary guidance block is proposed to help the network improve the segmentation performance. We believe that by adding this block, the network can learn more information at the boundary area, and the output of this block is integrated with the output of the backbone to guide the process of segmentation.

The proposed boundary guidance block (BGB) is shown as the light green box in Fig. 1, which is only applied on the low-level feature maps of VGG containing the sufficient boundary information. In practice, feature maps from the second layer of the first convolutional block in VGG (i.e. conv1–2) are used as the input of BGB. Our BGB consists of three dilated convolution kernels with different dilation rates, where dilated convolutions can control the receptive field and resolution without increasing the number of parameters. The generated feature maps are concatenated followed by a $1 \times 1$ convolutional layer to extract richer boundary information. As a result, let $d_r^s(f)$

denotes dilated convolution for feature $f$ with dilation rate $r$ and filter size of s × s. Our BGB can be expressed as:

$$F = conv_{1\times1}\Big(concat\Big(d_1^3(f), d_2^3(f), d_4^3(f)\Big)\Big) \tag{1}$$

### 3.2 Loss Function

The loss function is the most important component to train a deep learning neural network. In our loss function, not only the global pixel loss is considered but also the local contour loss. As to the global pixel loss, we utilize the widely used cross-entropy loss, which is implemented as:

$$L_{CE} = -\sum\nolimits_i \big(Y_i log Y_i^* + (1 - Y_i) log\big(1 - Y_i^*\big)\big), \tag{2}$$

where $Y_i$, $Y_i^*$ represent ground truth label and predicted probability value of pixel $i$. Besides, we propose a contour loss on the surrounding pixels of PPA to improve the poor performance around the edge. This local punishment forces the model pay more attention on the region where the more errors are going to happen. A weighted mask is obtained by dilation and erosion operations on the ground truth followed by a Gaussian filter, the purpose of this is to give more attention to the pixels closer to the boundary area, with the expression as follows:

$$M = Gauss\big(\big((Y; S)^+ - (Y; S)^-\big)\big), \tag{3}$$

where $(Y; S)^+$ and $(Y; S)^-$ represent dilation and erosion operations to the ground truth $Y$ respectively, and $S$ is the operation kernel size. The reason for Gaussian filtering is that pixels closer to the boundary should be given higher weights due to the high influence to the shape. The loss function of the boundary area consists of two parts: 1) the loss between the ground truth boundary area and the corresponding area of the output; 2) the loss between the BGB module output image and the ground truth boundary area. The loss function can be expressed as:

$$L_{contour} = \begin{array}{l} -\sum_i M_i\big(Y_i log Y_i^* + (1 - Y_i) log\big(1 - Y_i^*\big)\big) \\ -\sum_i \big(B_i log B_i^* + (1 - B_i) log\big(1 - B_i^*\big)\big) \end{array} \tag{4}$$

where $M_i$, $Y_i$ and $Y_i^*$ represent the mask, ground truth label and predicted probability value of pixel $i$ respectively, $B_i$, $B_i^*$ represent ground truth boundary label and BGB predicted probability value of pixel $i$. Finally, the total loss to train our model is:

$$L = L_{CE} + K \times L_{contour}, \tag{5}$$

where $K$ is a hyperparameter to balance the weights. In our experiments, $K$ is empirically set to 1.

# 4 Experiment and Results

## 4.1 Dataset and Evaluation

Retinal fundus PPA images can be divided into two categories: crescent-shaped and ring-shaped. In most cases, the shape of PPA is crescent-shaped, so we focus on the crescent-shaped PPA in our experiment. The dataset we use is provided by the Beijing Tongren Hospital, which contains 200 clinical data. For this dataset the PPA area is narrow which occupies an average of 2.37% of the ROI area and the age range of the data collectors is 6 to 14 years old. Because the target region is narrow, segmentation is difficult.

We randomly select 50 images as the testing set, and the rest as the training set. The preprocessing including eye alignment and ROI extraction is performed before resizing the images to a unified size of $512 \times 512$. Eye alignment mainly refers to the normalization of all data to the right eye. ROI extraction first uses the [15] method to locate the optic disc, and then the cropping side length is determined by 0.4 times the height of the fundus image.

We use F1-score and IOU as the main metrics to evaluate PPA segmentation performance. Both F1-score and IOU are metrics to measure the similarity between two sets. In the field of image segmentation, they are used to measure the similarity between the segmentation result and ground truth (GT). To evaluate the performance on the boundary, we apply Hausdorff distance as it is more sensitive to the boundary changes.

Our model is implemented using PyTorch. During training, our model is optimized using Adam optimizer with batch size of 8 and learning rate of 0.0001. The training stop condition adopts early stopping mechanism which selects the model with the smallest loss, if there is no lower point than the current point in the next 50 epochs, the current model is the final result. When constructing mask $M$ in contour loss, the kernel size $S$ is selected as $5 \times 5$, and the kernel size of the Gaussian filer is equal to $5 \times 5$.

## 4.2 Comparison with State-of-Arts

We compare our method with Li et al. [13], Unet [6], SegNet [7] and DRIU [11]. Figure 2 shows the visual comparison between our method and other methods. Our method achieves better results which are the closest to the ground truth especially on the boundaries. The reason for the analysis is that the method proposed in this paper adds boundary constraints, which makes the network pay more attention to boundary information in learning, thereby improving the performance of the entire network.

Table 1 show the quantitative results of our method and other methods on the clinical datasets. It can be observed from Table 1 that our method has an improvement in quantitative evaluation compared with other methods. Although Li's method [13] has superior performance in traditional methods, there is still a gap compared with the performance of algorithms based on deep learning.

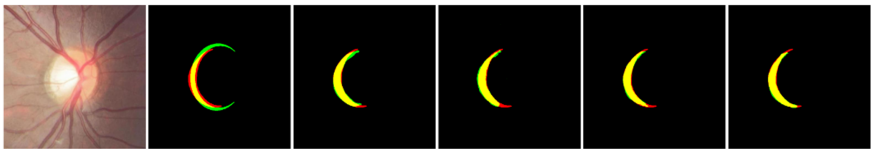


**Fig. 2.** Comparison with other methods. The corresponding number below the image is the F1-score corresponding to the result. In the result, the red is the ground truth, the green is the segmentation result, and the yellow is the overlap area. (Color figure online)

**Table 1.** Comparison with the-state-of-art methods.

| | Li et al. [13] | Unet [6] | SegNet [7] | DRIU [11] | Ours |
|---|---|---|---|---|---|
| F1-score | 63.70% | 79.11% ±0.70% | 76.57% ±1.25% | 79.43% ±0.67% | **80.06% ±0.39%** |
| Precision | 63.19% | **79.89% ±1.08%** | 75.71% ±1.45% | 78.69% ±1.16% | 79.06% ±0.86% |
| Recall | 68.13% | 79.67% ±1.15% | 79.42% ±1.16% | 81.57% ±0.33% | **82.25% ±0. 82%** |
| Accuracy | 97.93% | 99.01% ±0.04% | 98.86% ±0.06% | 99.01% ±0.05% | **99.04% ±0.02%** |
| IoU | 48.59% | 65.99% ±0.91% | 62.91% ±1.36% | 66.46% ±0.86% | **67.29% ±0.54%** |
| Hausdorff distance | 5.9699 | 5.7504 ±0.2489 | 5.8039 ±0.3182 | 5.5596 ±0.2154 | **5.4934 ±0.1384** |

### 4.3 Ablation Study

In order to validate the contribution of our BGB block and the contour loss, we have conducted the experiments on the models trained with or without each component. Table 2 summarizes the results of three models. We use DRIU and SegNet respectively as the baseline model. It can be seen from the results that whether the baseline uses DRIU or SegNet, the dataset has been greatly improved. For the dataset, the segmentation task is difficult for narrow PPA, mainly because narrow PPA occupies a small area in the image, which will be ignored without carefully loss design in deep learning. Adding only the BGB or CL module improves F1-score and IoU, but may cause the Hausdorff distance to decrease. The reason is that in addition to the boundary information being extracted and processed in the feature map generated by the BGB module, the blood vessels and optic disc regions will also be slightly affected. The CL focuses on the boundary area of the ground truth, so adding CL may cause discontinuities or holes in the segmentation. In such cases, the addition of BGB and CL can significantly improve the performance.

Take baseline method DRIU as an example, it can be seen from Fig. 3 that each added part has a certain constraint effect on the boundary.

**Table 2.** Ablation study on boundary guidance block and contour loss.

| | | Baseline | Baseline + BGB | Baseline + CL | Baseline + BGB + CL |
|---|---|---|---|---|---|
| DRIU | F1-score | 79.43% ±0.67% | 79.79% ±0.10% | 79.60% ±0.42% | **80.06% ±0.39%** |
| | IoU | 66.46% ±0.86% | 66.91% ±0.13% | 66.70% ±0.55% | **67.29% ±0.54%** |
| | Hausdorff distance | 5.5596 ±0.2154 | 5.6067 ±0.0891 | **5.4373 ±0.1366** | 5.4934 ±0.1384 |
| SegNet | F1-score | 76.57% ±1.25% | 76.72% ±1.17% | 76.94% ±2.04% | **77.16% ±1.04%** |
| | IoU | 62.91% ±1.36% | 63.00% ±1.40% | 63.23% ±2.58 | **63.50% ±1.29%** |
| | Hausdorff distance | 5.8039 ±0.3182 | 6.0630 ±0.2331 | 5.9227 ±0.4811 | **5.6910 ±0.1638** |

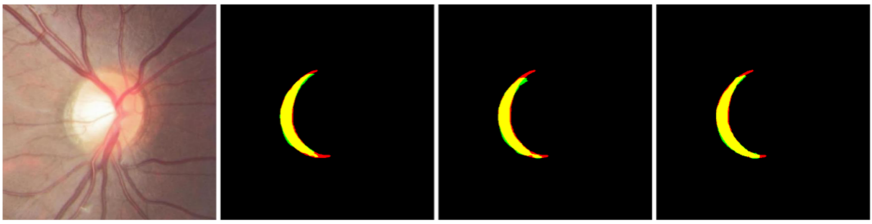


**Fig. 3.** Comparison of the ablation study with DRIU baseline method. Corresponding number below the image is the Hausdorff distance corresponding to the result. In the result, the red is the ground truth, the green is the segmentation result, and the yellow is the overlap area. (Color figure online)

## 5 Conclusion

In this paper, we propose a deep convolution neural network to segment PPA area automatically from retinal images. To solve the problem of irregular and blurry boundaries of PPA, we propose a boundary guidance block and introduce a contour loss to improve the PPA segmentation performance on the boundary. The proposed model is trained and evaluated based on clinical data. Our model achieves 80.06% F1-score, 67.29% IoU, Hausdorff distance of 5.4934, outperforming the state-of-art model. In the future, we will further analyze multiple situations of PPA such as ring-shaped area.

**Acknowledgment.** The research work is supported by the National Natural Science Foundation of China (NSFC) (Grant No. 82072007) and China Postdoctoral Science Foundation (No. 2020M680387).

## References


1. Manjunath, V., Shah, H., Fujimoto, J.G., Duker, J.S.: Analysis of peripapillary atrophy using spectral domain optical coherence tomography. Ophthalmology **118**(3), 531–536 (2011)
2. Jonas, J.B., Gusek, G.C., Naumann, G.O.H.: Optic disk morphometry in high myopia. Graefe's Arch. Clin. Exp. Ophthalmol. **226**(6), 587–590 (1988)
3. Lu, C.K., Tang, T.B., Alan, F.M., Lauda, A., Dhillon, B.: Automatic parapapillary atrophy shape detection and quantification in colour fundus images. In: 2010 Biomedical Circuits and Systems Conference (BioCAS), pp. 86–89. Paphos (2010)
4. Patil, D.D., Deore, S.G.: Medical image segmentation: a review. Int. J. Comput. Sci. Mob. Comput. **2**(1), 22–27 (2013)
5. Narkhede, H.P.: Review of image segmentation techniques. Int. J. Sci. Modern Eng. **1**(8), 54–61 (2013)
6. Ronneberger, O., Fischer, P., Brox, T.: U-Net: convolutional networks for biomedical image segmentation. In: International Conference on Medical Image Computing and Computer-Assisted Intervention, pp. 234–241. Springer, Cham (2015)
7. Badrinarayanan, V., Kendal, A., Cipolla, R.: SegNet: a deep convolutional encoder-decoder architecture for image segmentation. IEEE Trans. Pattern Anal. Mach. Intell. **39**(12), 2481–2495 (2017)
8. Joshi, G.D., Sivaswamy, J., Krishnadas, S.R.: Optic disk and cup segmentation from monocular color retinal images for glaucoma assessment. IEEE Trans. Med. Imag. **30**(6), 1192–1205 (2011)
9. Yu, H., et al.: Fast localization and segmentation of optic disk in retinal images using directional matched filtering and level sets. IEEE Trans. Inform. Technol. Biomed. **16**(4), 644–657 (2012)
10. Bharkad, S.: Automatic segmentation of optic disk in retinal images. Biomed. Signal Process. Control **31**, 483–498 (2017)
11. Maninis, K.-K., Pont-Tuset, J., Arbeláez, P., Van Gool, L.: Deep Retinal Image Understanding. In: Ourselin, S., Joskowicz, L., Sabuncu, M.R., Unal, G., Wells, W. (eds.) Medical Image Computing and Computer-Assisted Intervention – MICCAI 2016, pp. 140–148. Springer International Publishing, Cham (2016). https://doi.org/10.1007/978-3-319-46723-8_17
12. Wang, L., Liu, H., Lu, Y., Chen, H., Zhang, J., Pu, J.: A coarse-to-fine deep learning framework for optic disc segmentation in fundus images. Biomed. Signal Process. Control **51**, 82–89 (2019)
13. Li, H., Li, H., Kang, J., Feng, Y., Xu, J.: Automatic detection of parapapillary atrophy and its association with children myopia. Comput. Methods Programs Biomed. **183**, 105090 (2020)
14. Chai, Y., Liu, H., Xu, J.: A new convolutional neural network model for peripapillary atrophy area segmentation from retinal fundus images. Appl. Soft Comput. J. **86**, 1–11 (2020)
15. Li, H., et al.: Automatic location of optic disk in retinal images. In: Proceedings 2001 International Conference on Image Processing, vol. 2, pp. 837–840 (2001)